Shallow Water Propagation

William L. Siegmann
Rensselaer Polytechnic Institute
110 Eighth Street
Jonsson-Rowland Science Center 1C08
Troy, New York 12180-3590
phone: (518) 276-6905 fax: (518) 276-2825 email: siegmw@rpi.edu

Adam M. Metzler
Rensselaer doctoral student

Kara G. McMahon
Rensselaer doctoral student

Award Numbers: N000140410016
N000140810972 (Ocean Acoustics Graduate Traineeship)
N000140910638 (Ocean Acoustics Graduate Traineeship)
http://www.math.rpi.edu/www/ocean_acoustics

LONG-TERM GOALS

Develop methods for deterministic and stochastic acoustic calculations in complex shallow water environments, specify their capabilities and accuracy, and apply them to explain experimental data and understand physical mechanisms of propagation.

OBJECTIVES

(A) Treat propagation from narrowband and broadband sources over elastic and poro-elastic sediments, and incorporate realistic bathymetric, topographic, and geoacoustic variations.

(B) Quantify acoustic interactions with physical features in the ocean volume and with geoacoustic features of the ocean sediment, and analyze and interpret experimental data.

APPROACH

(A) Develop efficient and accurate parabolic equation (PE) techniques for propagation through heterogeneous sediments. Treat range dependence and sediment layering by single scattering and energy conservation methods. Benchmark results using data and special high-accuracy solutions.

(B) Construct representations for ocean environmental and geoacoustic variability using data and parametric models. Determine acoustic fields with PE, normal mode, and other approximation methods. Use experimental data and computational results to assess propagation mechanisms.

Report Documentation Page

Form Approved
OMB No. 0704-0188

1. REPORT DATE	2. REPORT TYPE	3. DATES COVERED
SEP 2011		**00-00-2011 to 00-00-2011**

4. TITLE AND SUBTITLE	5a. CONTRACT NUMBER
Shallow Water Propagation	5b. GRANT NUMBER
	5c. PROGRAM ELEMENT NUMBER
6. AUTHOR(S)	5d. PROJECT NUMBER
	5e. TASK NUMBER
	5f. WORK UNIT NUMBER
7. PERFORMING ORGANIZATION NAME(S) AND ADDRESS(ES) **Rensselaer Polytechnic Institute,110 Eighth Street,Jonsson-Rowland Science Center 1C08,Troy,NY,12180-3590**	8. PERFORMING ORGANIZATION REPORT NUMBER
9. SPONSORING/MONITORING AGENCY NAME(S) AND ADDRESS(ES)	10. SPONSOR/MONITOR'S ACRONYM(S)
	11. SPONSOR/MONITOR'S REPORT NUMBER(S)

12. DISTRIBUTION/AVAILABILITY STATEMENT
Approved for public release; distribution unlimited

13. SUPPLEMENTARY NOTES

14. ABSTRACT

15. SUBJECT TERMS

16. SECURITY CLASSIFICATION OF:			17. LIMITATION OF ABSTRACT	18. NUMBER OF PAGES	19a. NAME OF RESPONSIBLE PERSON
a. REPORT **unclassified**	b. ABSTRACT **unclassified**	c. THIS PAGE **unclassified**	**Same as Report (SAR)**	**13**	

- Principal collaborators are: Rensselaer PhD students, Dr. Michael Collins (NRL), Profs. William Carey and Allan Pierce (BU), Drs. James Lynch, Timothy Duda, and Ying-Tsong Lin (WHOI), and recent Rensselaer PhD graduates.

WORK COMPLETED

(A) Propagation model development

(1) ***New capabilities for range-dependent elastic sediments***

- High fidelity data from propagation over an elastic slab with variable bottom slope in a large NRL tank validates the accuracy [1] of a new PE method designed for problems with range-dependent bathymetry, variable thickness sediment layers, and topographic variations for beach, island, and coastal problems.
- Additional verification of the method accuracy is obtained by comparing results with benchmarks for environments with large sound speeds changes or with waves on range-dependent elastic interfaces [2], and guidelines for choosing computational parameters are provided.
- Introducing new propagation variables that are based on quantities conserved across interfaces produces a reformulation [3] that has potential of treating range-dependent bathymetry and elastic interfaces more efficiently and accurately than currently available methods.
- Range-dependent transversely isotropic elastic sediments, which are a feature of many coastal regions, are treated by another new formulation that enables evaluation of the relative significance of anisotropic effects on propagation [4].

(2) ***Accurate calculations for poro-elastic sediments***

- An initial propagation model that can treat weak range dependence in transversely isotropic poro-elastic sediments demonstrates that PE methods are feasible for these environments [5], and also indicates the influence of anisotropy.
- Propagation variables and computational techniques currently used for elastic sediments [2] are generalized to poro-elastic environments, and results from benchmark cases show improved accuracy and increased capabilities for multi-layered sediments [6].
- Another method for poro-elastic media [7], based on an extension of the elastic-variable reformulation [3], shows accurate results for range-independent problems and suggests similar advantages of efficiency and accuracy for range-dependent environments.

(B) Propagation mechanism assessment

(1) ***Nonlinear internal wave effects***

- When an acoustic mode propagate adiabatically across a nonlinear internal wave (NIW) at small incident angles with the wave front, the interaction may produce horizontal Lloyd mirror interference patterns [8], as were predicted by others and observed recently, and the patterns have especially interesting features when the NIW front has curvature.
- Characteristic parameters of NIWs are estimated from satellite SAR images using edge identification and related techniques [9] in order to obtain improved predictions of their acoustic effects, and parameter estimates are validated by comparisons with mooring and other available data.
- A modal transport theory is used to develop a scattering model for acoustic energy inside a NIW duct [10] in which wave front segments are treated as scattering elements, and a modified diffusion equation describes the evolution of a grid-averaged intensity in the duct.
- Calculations from the modal transport theory are used to determine the influence of NIW parameter variations, background environmental conditions, and acoustic parameters on averaged intensity [11], and results are compared and benchmarked with propagation computations.

(2) ***Modal attenuation coefficient variability***

- A physical interpretation of the effects of nonlinear frequency dependence of sediment attenuation is developed by employing a parametric description for a Perkeris waveguide [12] and determining the frequency behavior of modal attenuation coefficients.
- Based on acoustic data from the Gulf of Mexico, new results for modal attenuation coefficient values are found after identifying and using a relevant set of measured sound speed profiles [13], confirming the validity of some of the estimates that were obtained previously by curve fitting.
- The strength and water-column location of sound speed gradients are shown to have very different effects on the parametric dependence of modal attenuation coefficients [14], particularly their frequency dependence, by using improved modal asymptotic approximations.

(3) ***Transmission loss dependence on intrinsic sediment attenuation***

- The overall linear attenuation of averaged reduced transmission loss is related to the frequency dependence of modal attenuation coefficients [15], by quantifying the principal dependence on features of the water sound speed profile.

- Efficient tools are constructed to find relationships between the frequency power law of intrinsic attenuation, modal attenuation coefficients, and averaged transmission loss [16] at recent experimental sites, and the robustness of earlier power law estimates is evaluated.
- Relatively straightforward formulas for averaged transmission loss in range-independent waveguides are derived from mode theory, and they reduce to well-known results of Rogers and others at high frequencies and for either isospeed or constant-gradient water sound speed profiles [17].

(4) ***Card-house theory of mud structure***

- One feature of this model is the presence of electric charges on bubbles, and under uniform conditions it is found that charged bubbles are required to be non-spherical [18], which has been observed in laboratory experiments and is anticipated for mud in situ.
- Another key component is that based on chemical, electrical, and material structure, mud platelets are hypothesized to behave like electric quadrupoles, and an estimate of shear wave speed is obtained by computing the oscillation frequency of a hinged joint formed by platelets which interact end to side [19].
- The shear speed estimate is extended to account for platelet interactions in which the interaction is modeled as a cantilevered beam rather than a hinged joint [20], and estimates are in accord with the low shear speed values found in high-porosity mud sediments.

RESULTS (from two selected investigations)

(A) An essential capability for ocean acoustic data analysis and other applications is efficient and accurate propagation calculations in shallow water waveguides with range-dependent poro-elastic sediment layers. Porosity and elasticity are important because energy transfer between compressional and shear modes may produce significant acoustic intensity and phase changes. In addition attenuation may increase substantially because of physical mechanisms in these sediments. A critical computational challenge is that wave number energy spectra for poro-elastic sediments are much broader than for fluid models. Our approach is based on the Biot poro-elastic theory, which is the most common model for ocean sediments. The only previous poro-elastic PE is over a decade old, and although it was extended to include sediment anisotropy [5], its computational capabilities are relatively limited. It is important that recent progress for elastic sediments be generalized to layered poro-elastic media. For example, benchmarking provides necessary validation for the elastic method, and one paper [1] shows applications to high quality data obtained from an NRL experimental series using elastic slabs. Additional calculations [2] show excellent agreement with benchmarks for problems with even relatively large changes in sound speeds and with range-dependent interface waves. The new elastic methods were developed from a series of advances: formulating with different dependent variables, employing coordinate rotations at range locations of bathymetry slope changes, and improved range-dependent corrections at stair-step approximations of changes in sediment, ocean, and interface parameters. The starting point is to focus on range-independent sediment

layers and to generalize the dependent variables (denoted by $\tilde{q}$) in the original poro-elastic PE using state of the art elastic results. ***Figure 1*** illustrates the accuracy and capability of the initial version of our method. The top row shows calculations of transmission loss at depth 50 m in an environment with a 100 m ocean layer over one deep poro-elastic layer. The left panel shows good agreement between the transmission loss using the $\tilde{q}$ variables and a benchmark calculated from the wave number integration code OASIS. The right panel illustrates that the PE calculations using the new variables (denoted by $\hat{q}$) match those using $\tilde{q}$ for this single-layer environment [6]. In contrast, the middle row shows calculations for this environment with a new 20 m thick poro-elastic upper sediment layer included. The left panel shows that the calculations using $\tilde{q}$ disagree from the benchmark both quantitatively and also qualitatively, since the PE results tend to a three-mode pattern while the benchmark tends to a two-mode pattern. However, the right panel shows that calculations using $\hat{q}$ agree with the benchmark pattern and have relatively smaller amplitude differences. The bottom panel compares the compressional wave portion of the horizontal wave number spectra of the $\tilde{q}$ and $\hat{q}$ solutions for the two-layer environment of the middle row. The leftmost peak in the spectra corresponds to the wave in the lower poro-elastic layer. The difference in peak amplitudes is the source of the qualitative change between results from the two methods in the middle row. From these and other calculations, we conclude that the $\hat{q}$ solution, unlike the $\tilde{q}$ solution, can handle propagation through multi-layered poro-elastic environments.

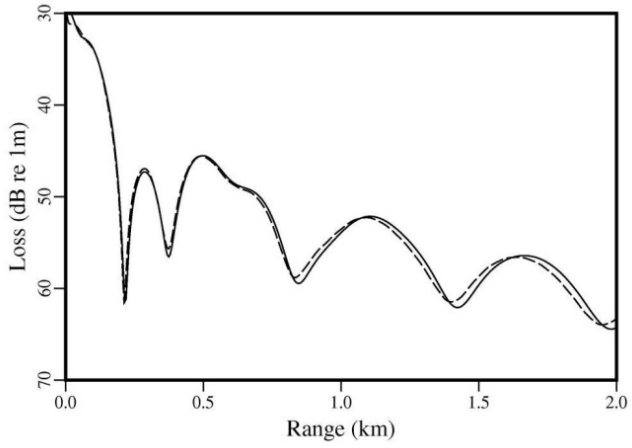
Loss (dB re 1m)
30
40
50
60
70
0.0
0.5
1.0
1.5
2.0
Range (km)

(a)

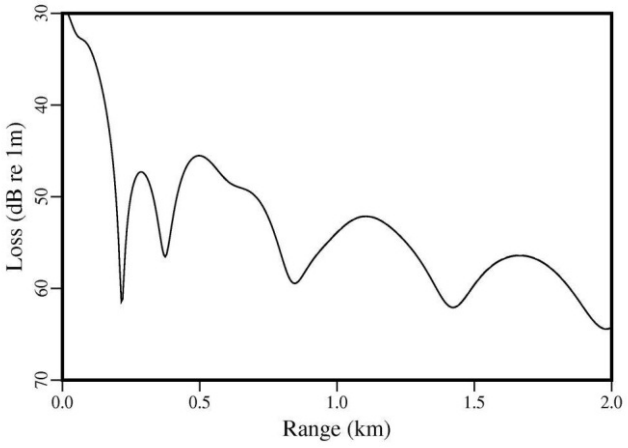
Loss (dB re 1m)
30
40
50
60
70
0.0
0.5
1.0
1.5
2.0
Range (km)

(b)

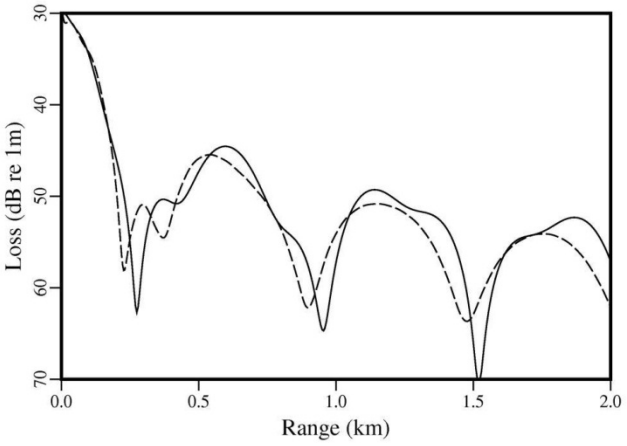
Loss (dB re 1m)
30
40
50
60
70
0.0
0.5
1.0
1.5
2.0
Range (km)

(c)

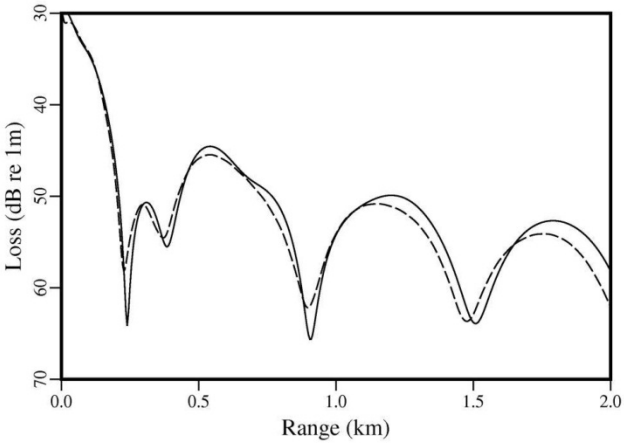
Loss (dB re 1m)
30
40
50
60
70
0.0
0.5
1.0
1.5
2.0
Range (km)

(d)

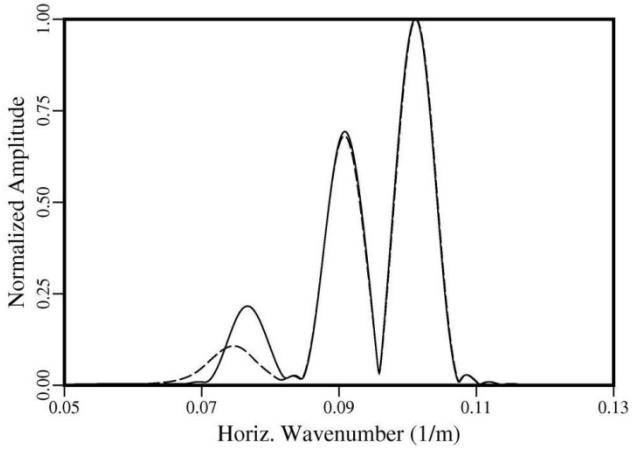
Normalized Amplitude
0.00
0.25
0.50
0.75
1.00
0.05
0.07
0.09
0.11
0.13
Horiz. Wavenumber (1/m)

(e)

Figure 1 (above). Improved calculation of propagation in poro-elastic sediments follows from an appropriate formulation of physical variables in the PE method. Transmission loss (TL) curves (dB re: 1 m) are shown between 30 and 70 dB along a 2 km track which is 50 m below the upper surface, for a 25 Hz source at 25 m depth.

Fig. 1(a): A range-independent benchmark environment consists of a 100 m isospeed ocean with c_w = 1500 m/s which overlies a deep poro-elastic sediment layer. The geoacoustic parameters of the sediment are density ρ_s = 2.0 gm/cm^3, porosity α = 0.15, sound speeds c_{p1} = 2040 m/s, c_{p2} = 1250 m/s, and c_s = 700 m/s, and attenuations β_{p1} = 0.3 dB/λ , β_{p2} = 15 dB/λ , and β_s = 2.5 dB/λ . The value of β_{p2} reflects higher attenuation for the Biot slow compressional wave. The solid curve is calculated from an earlier formulation with dependent variables $\tilde{q}$ = (Δ, w, ζ). The dashed curve is calculated from the wave number integration implementation OASIS. Both curves agree well and tend toward a two-mode propagation pattern with a wavelength of about 500 m. Fig. 1(b): Same environment as Fig. 1(a). The dashed curve is from a new formulation with variables $\hat{q}$ = (u_x , w, ζ), which generalizes a successful elastic-media method. The two curves are visually identical.

Fig. 1(c): Another range-independent benchmark environment has the same ocean and deep poro-elastic layers as Figs. (a) and (b) but with a second 20 m thick poro-elastic layer between them. The geoacoustic parameters of the upper sediment layer are density ρ_s = 2.0 gm/cm^3, porosity α = 0.2, sound speeds c_{p1} = 1850 m/s, c_{p2} = 1250 m/s, and c_s = 600 m/s, and attenuations β_{p1} = 0.3 dB/λ , β_{p2} = 10 dB/λ , and β_s = 0.5 dB/λ . The solid curve is the solution with variables $\tilde{q}$; the dashed curve is the solution from OASIS. The two curves have significant amplitude differences, and the limiting solution behaviors are different: a three-mode pattern from the PE, and a two-mode pattern from OASIS. Fig. 1(d): Same two-layer sediment environment as Fig. 1(c). Here the solid curve is the solution with variables $\hat{q}$; the dashed curve is the solution from OASIS. The two solutions agree well in pattern with small amplitude differences.

Fig. 1(e): For the same environment as Figs. 1(c) and 1(d), horizontal wave number spectra between 0.06 and 0.12 /m and normalized with maximum-peak amplitude one are compared for the $\tilde{q}$ and $\hat{q}$ solutions. The three main peaks in this portion of the spectrum, from right to left, correspond to c_w in the water, c_{p1} in the upper poro-elastic layer, and c_{p1} in the lower poro-elastic layer. The left-most peak for the $\tilde{q}$ solution is sufficiently large for the TL to approach a three-mode pattern over the 2 km range, while the corresponding peak for the $\hat{q}$ solution is sufficiently small for a two-mode TL pattern. The incorrect energy distribution in the lower poro-elastic sediment layer causes inaccurate results for the $\tilde{q}$ solution. From these and other calculations, we conclude that the $\hat{q}$ solution is efficient and has the capability for propagation calculations in multi-layered poro-elastic environments.

(B) The widespread occurrence of NIWs in shallow ocean regions led to intensive experimental study for nearly two decades, to determine how, when, and where they may cause significant changes in acoustic signals. In particular, results from SW06 display many phenomena for which important modeling capabilities and theoretical understanding have been developed. As only one example, the mechanism for the creation of an interference pattern in coherent acoustic propagation near the leading crest of a NIW train was conjectured as a horizontal Lloyd mirror. Recently these striking patterns have been observed in SW06 data. Modeling studies show the dependence of the mirror pattern on source-receiver geometry as well as front shape and structure parameters, especially large-scale wave front curvature [8]. One research issue is to improve the estimates for NIW parameters by assimilating all types of available data, especially ocean surface SAR images [9]. In addition to deterministic propagation modeling, the ubiquity and variability of NIWs suggests that stochastic modeling has an important role for estimating their acoustic effects. Itwould be valuable to develop calculation tools for readily clarifying the physical propagation mechanisms occurring in NIWs, as well as to provide robust estimates efficiently for acoustic quantities of interest. The availability of fully three-dimensional PEs is essential to benchmark the tools and provide confidence in their application. Acoustic energy traveling through and interacting with a NIW duct, which may be straight, curved, terminating, or intersecting others, is a situation of high oceanic, experimental, and computational interest. Consequently, our approach focuses initially on one part of this process. Adiabatic vertical-mode propagation is assumed, and segments of NIW fronts in the duct are treated as scattering elements. As suggested by our WHOI colleagues, one can visualize the acoustic wave interacting with the NIW front elements like a Galton's box with discrete scatterers. Proceeding from this idea, along with appropriate scale and other constraints, a radiative-transport model can be constructed [10] for vertical modes. A fundamental result for the locally-averaged acoustic intensity is a modified diffusion equation, from which predictions can be determined across and down the duct. At the left of the top row of ***Figure 2*** is a SAR image with many interacting NIW trains, and the middle panel is an expanded portion. The key feature is the structure of the train, proceeding from basically coherent fronts in the forward third, to broken wave crests in the middle third, and to generally diffuse scatterers in the rear third. Based on examinations of many SAR images, a reasonable model for a NIW train with straight wave fronts is illustrated in the schematic on the right. The middle row shows averaged acoustic intensity for a "baseline" duct that is filled with a train of NIWs, each of which has coherent, unbroken wave fronts. A small amount of diffuse scattering is assumed to occur between each of the NIWs. The left panel shows a symmetric transmission loss pattern, given the source position, and the region of higher loss expands toward the duct boundaries as distance increases from the source. The right panel shows the difference in loss from the case with no NIWs. Their effect on averaged intensity ranges up to 6 dB for this baseline case. The bottom row shows averaged intensity for the environment in the schematic Fig. 2(c), which more faithfully models NIW fronts in the ocean. The upper portions of both panels show the expected correspondence with the upper portions of the middle-row panels, with changes again up to 6 dB. Compared with the middle-row panels, the lower portions of both bottom-row panels show distinctly less loss because of the weaker scattering toward the rear of the train. A visible loss difference near the center axis occurs between the right panels of the middle and bottom rows. We conclude from these example environments and others that locally-averaged intensity in NIW ducting environments can be readily obtained from the modal-transport model. Future work will focus on benchmarking the results and examining other typical shallow water NIW environments.

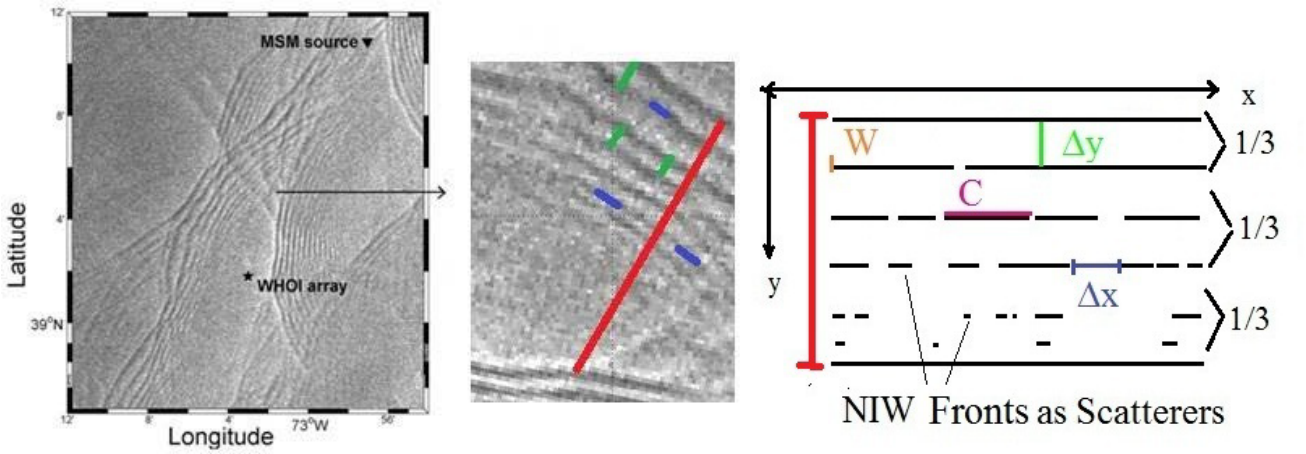
MSM source
WHOI array
Latitude
Longitude
39°N
73°W
x
y
W
Δy
C
Δx
1/3
1/3
1/3
NIW Fronts as Scatterers

(a) **(b)** **(c)**

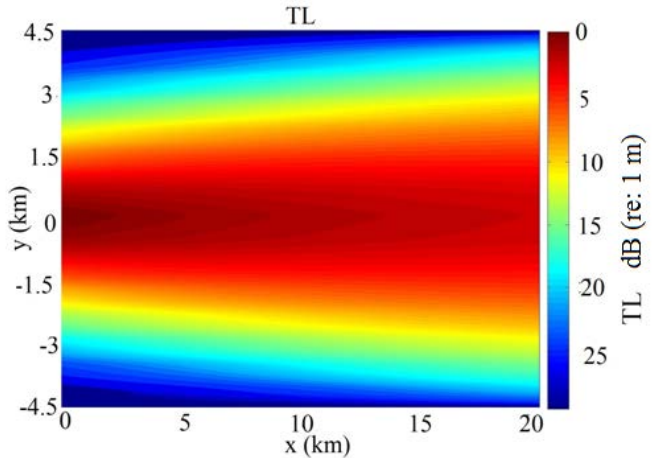
TL
y (km)
x (km)
TL dB (re: 1 m)

(d)

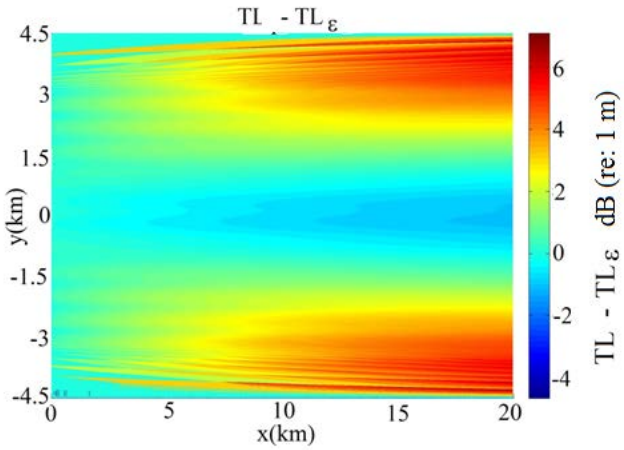
TL - TLε
y(km)
x(km)
TL - TLε dB (re: 1 m)

(e)

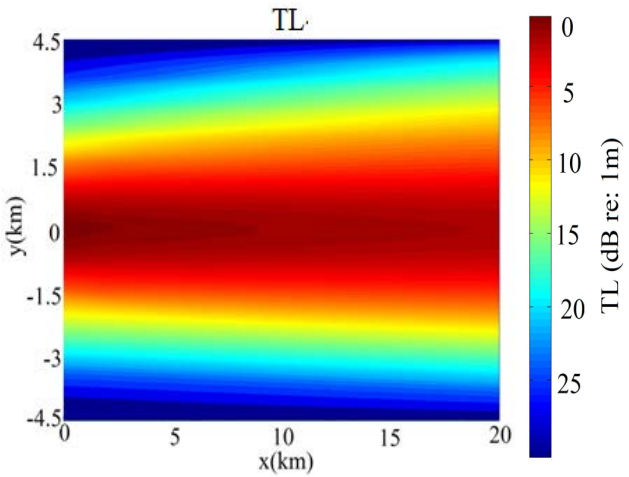
TL
y(km)
x(km)
TL (dB re: 1m)

(f)

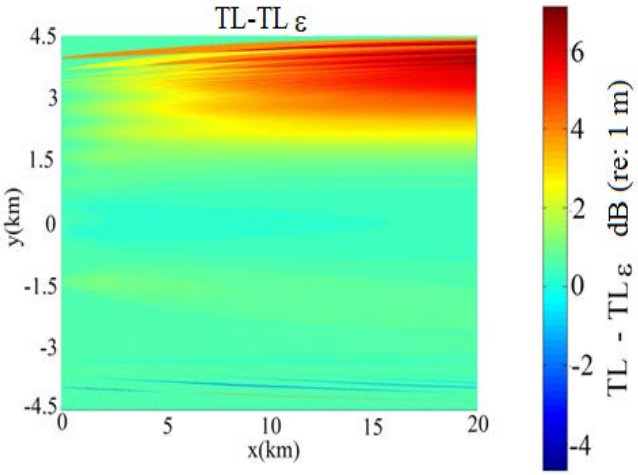
TL-TLε
y(km)
x(km)
TL - TLε dB (re: 1 m)

(g)

Figure 2 (above): *Nonlinear internal wave (NIW) ducts cause horizontal scattering of vertical modes. Averaged acoustic intensity calculations using a modified horizontal diffusion equation show the scattering characteristics.* ***Fig. 2(a)*** *is a synthetic aperture radar (SAR) image near 39° N, 72° W from the SW06 experiment, showing multiple traveling trains of NIW fronts that vary from coherent (lead of train) to broken (rear of train).* ***Fig. 2(b)*** *is a magnified portion of the SAR image that suggests positions of NIW scatterers. Red line indicates the duct width between two coherent NIWs which lead nearby wave trains; green lines indicate spaces Δy between NIW fronts in the train; and blue lines are spaces Δx between along-crest segments of broken wave fronts.*

Fig. 2(c) *is a schematic of a NIW duct with wave fronts modeled as linear. Coordinates x (and y) are along (and across) wave crests, and the schematic corresponds to rotating Fig. 2(b) about 45° counterclockwise. In addition to Δx and Δy, other parameters are length C of along-crest segments (magenta) and NIW cross-crest widths W (orange). Based on an ensemble of SAR images, the duct is best modeled with three regions in y; $\Delta x = 0$ in the forward third, $\Delta x > 0$ in the middle third (average value 0.46 km), and diffuse scatterers in the rear third. SAR images provide an average value of 0.63 km for Δy but do not resolve W, for which wave speed data gives an average value as 0.4 km.*

Fig. 2(d) *shows averaged acoustic intensity for a duct environment with one train of NIW scatterers. In this example the train fills the entire duct, with each coherent NIW having unbroken wave crests as suggested by the forward third of Fig. 2(c). Each NIW is modeled as a boxcar function, and all constant spacings Δy and widths W are the average values. The scattering strength between waves is a small fraction ε of the strength inside waves, in order to account for diffuse scattering which is inevitably present. For a source at the coordinate origin, color contours of reduced transmission loss (TL) (dB re: 1 m) from 0 to 25 dB are shown over 20 km range and the full duct width 9 km. Symmetrically about y = 0, a strong central TL "beam" appears in the middle third of the picture, and the beam spread increases with x because the NIWs cause scattering and energy defocusing.* ***Fig. 2(e):*** *Contours of TL difference, with dynamic range about 10 dB, between Fig. 2(d) and the case with no NIWs present (diffusive scattering everywhere). The largest differences are within 2 km of the duct boundaries and beyond 10 km range. These regions receive little energy with no NIWs and considerably more with NIWs from scattering, producing up to 6 dB differences in averaged intensity.*

Fig. 2(f) *has TL contours like those in Fig. 2(d) but for a duct environment with a train of NIW scatterers with fronts of varying coherence. As in Fig. 2(c), the forward third has unbroken crests; the middle third has broken fronts, with value C = 2.15 km chosen from within the range of observations; and the rear third has only diffuse scatterers. The internal wave model and other parameter values are the same as for Fig. 2(d). For values of y below the source, the TL "beam" is more focused because scatterers are weaker or absent. Above the source the "beam" spreads as in Fig. 2(d) because of the stronger scatterers.* ***Fig. 2(g)*** *has contours of average TL difference like those in Fig. 2(e). The largest differences, again about 6 dB, are above the source because the NIWs scatter energy into that region. In contrast to the coherent fronts used for Fig. 2(e), broken fronts in the middle third produce weaker scattering, comparable to the diffusive scattering regime. A scattering approximation for NIW effects using a modified diffusion equation shows how and where environmental variability can produce significant averaged TL differences.*

IMPACT/APPLICATIONS

New or enhanced capabilities are provided for propagation predictions that depend on physical properties of shallow water sediments, including layering, elasticity, porosity, and anisotropy. Range-dependent variability from bathymetry, topography, and sediment layer interfaces in propagation calculations can be treated. Intensity attenuation and coherence statistics that result from environmental fluctuations and other experimental variability can be found more efficiently. Data analyses and model comparisons allow specification for application purposes of the relative significance of key physical mechanisms: linear versus nonlinear frequency dependence of sediment attenuation, sediment heterogeneity versus homogeneity, water column versus bathymetric variability, water column scattering versus refraction, and vertical versus horizontal mode coupling due to internal solitons and bathymetry. Results from modeling and data analyses of experiments, particularly the New Jersey Shelf and the ACT experimental series, are partly aimed toward improving shallow water sonar systems and predictions. Propagation model implementations, analysis tools, and data representation techniques are distributed to university, laboratory, and research/development groups.

RELATED PROJECTS

- Continuing projects with Dr. Michael Collins [4]-[7] also include a monograph on new parabolic wave equation models and applications [22], for which the principal research results are nearly complete and chapter drafts are prepared.

- In addition to investigations with Drs. James Lynch and Timothy Duda and their colleagues [8]-[11] of propagation effects from waveguides of variable structure generated by nonlinear internal waves, a related project characterizes whispering gallery and other modes [21].

- Research with Profs. William Carey and Allan Pierce [12]-[20] focuses on propagation variability from sediment geoacoustic structure and attenuation, with recent emphasis on quantifying predictions from their theory of mud structure and acoustics.

REFERENCES

[1] H. J. Simpson, J. M. Collis, R. J. Soukup, M. D. Collins, and W. L. Siegmann, "Experimental testing of the variable rotated elastic parabolic equation." Accepted for publication in *J. Acoust. Soc. Am*.

[2] A. M. Metzler, W. L. Siegmann, M. D. Collins, and J. M. Collis, "Elastic media propagation including Rayleigh waves with the single-scattering parabolic equation." Accepted for publication in the *J. Acoust. Soc. Am*. Supported by OA Graduate Traineeship Award 0972.

[3] M. D. Collins and W. L. Siegmann, "Improving the parabolic equation solution for solutions involving sloping fluid-elastic interfaces," (A) *J. Acoust. Soc. Am*. **127**, 1962 (2010).

[4] A. M. Metzler, W. L. Siegmann, R. N. Baer, M. D. Collins, and J. M. Collis, "Parabolic equation solutions for anisotropic waves in heterogeneous media." See also (A) *J. Acoust. Soc. Am*. **125**, 2500 (2009). In preparation for submission. Supported by OA Graduate Traineeship Award 0972.

[5] A. J. Fredricks, W. L. Siegmann, and M. D. Collins, "Parabolic equation models for anisotropic poro-elastic media." Submitted for refereed publication.

[6] A. M. Metzler, W. L. Siegmann, and M. D. Collins, "Improving the parabolic equation solution for problems involving poro-elastic media." See also (A) *J. Acoust. Soc. Am*. **127**, 1962 (2010). Submitted for refereed publication. Supported by OA Graduate Traineeship Award 0972.

[7] A. M. Metzler and W. L. Siegmann, "Parabolic equation solutions with increased capabilities for layered poro-elastic media." See also (A) *J. Acoust. Soc. Am*. **128**, 2479 (2010). Submitted for refereed publication. Supported by OA Graduate Traineeship Award 0972.

[8] K. G. McMahon, L. K. Reilly-Raska, W. L. Siegmann, J. F. Lynch, and T. F. Duda, "Horizontal Lloyd Mirror patterns from straight and curved nonlinear waves." Accepted for publication in *J. Acoust. Soc. Am*. Supported by OA Graduate Traineeship Award 0638.

[9] C. C. Boughan Khan, T. F. Duda, J. F. Lynch, A. E. Newhall, and W. L. Siegmann, "Nonlinear internal wave parameter extraction from SAR images." In preparation for submission.

[10] K. G. McMahon, J. F. Lynch, Y.-T. Lin, N. Xiang, and W. L. Siegmann, "Energy propagation in nonlinear internal wave ducts from radiative transport theory." See also (A) *J. Acoust. Soc. Am*. **128**, 2335 (2010). In preparation for submission. Supported by OA Graduate Traineeship Award 0638.

[11] K. G. McMahon, J. F. Lynch, Y.-T. Lin, and W. L. Siegmann, "Nonlinear internal wave parameter influences on energy propagation using radiative transport theory." See also (A) *J. Acoust. Soc. Am*. **129**, 2458 (2011). In preparation for submission. Supported by OA Graduate Traineeship Award 0638.

[12] W. J. Saintval, A. D. Pierce, W. M. Carey, and W. L. Siegmann, "A modified Pekeris waveguide for examining sediment attenuation influence on modes." Submitted for refereed publication.

[13] W. J. Saintval, W. L. Siegmann, W. M. Carey, and A. D. Pierce, "Parameter sensitivities of modal attenuation coefficients for sandy sediments in the Gulf of Mexico." Submitted for refereed publication.

[14] S. V. Kaczkowski, W. L. Siegmann, A. D. Pierce, and W. M. Carey, "Parametric variations of modal attenuation coefficients obtained from modal approximations." In preparation for submission.

[15] W. J. Saintval, W. L. Siegmann, W. M. Carey, A. D. Pierce, and J. F. Lynch, "Estimation of effective attenuation coefficients from the New Jersey Shelf environment." In preparation for submission.

[16] S. V. Kaczkowski, W. J. Saintval, W. M. Carey, A. D. Pierce, and W. L. Siegmann, "Relationships between intrinsic sediment attenuation, modal attenuation, and transmission loss in experimental environments over sandy-silty sediments." See also (A) *J. Acoust. Soc. Am*. **126**, 2167 (2009). In preparation for submission.

[17] S. V. Kaczkowski, W. M. Carey, A. D. Pierce, and W. L. Siegmann, "Averaged transmission loss expressions in shallow water waveguides with sandy-silty sediments." See also (A) *J. Acoust. Soc. Am*. **128**, 2480 (2010). In preparation for submission.

[18] J. O. Fayton, A. D. Pierce, W. M. Carey, and W. L. Siegmann, "The card-house structure of mud: energy between particles and its effect on bubble formation." See also (A) *J. Acoust. Soc. Am*. **127**, 1938 (2010). In preparation for submission.

[19] J. O. Fayton, A. D. Pierce, W. M. Carey, and W. L. Siegmann, "The card-house structure of mud: determination of shear wave speed." See also (A) *J. Acoust. Soc. Am*. **128**, 2357 (2010). In preparation for submission.

[20] J. O. Fayton, A. D. Pierce, W. M. Carey, and W. L. Siegmann, "Estimation of the shear wave speed in mud based on a card-house theory with elastic platelets." See also (A) *J. Acoust. Soc. Am*. **129**, 2389 (2011). In preparation for submission.

[21] Y.-T. Lin, K. G. McMahon, W. L. Siegmann, and J. F. Lynch, "Acoustic modes in a curved internal wave duct." See also (A) *J. Acoust. Soc. Am*. **130**, xxxx (2011). In preparation for submission.

[22] M. D. Collins and W. L. Siegmann, *Parabolic Wave Equations with Applications*. In preparation for Springer-Verlag publishers.

PUBLICATIONS

- Accepted [refereed]: [1], [2], [8]
- Submitted [refereed]: [5], [6], [7], [12], [13]